

## Accurate calculation of three-body depletion interactions

Dave Goulding and Simone Melchionna

*Department of Chemistry, University of Cambridge, Lensfield Road, Cambridge CB2 1EW, United Kingdom*

(Received 23 January 2001; published 13 June 2001)

We compute three-body depletion interactions in a hard-sphere mixture within the framework of density-functional theory and by considering the infinite dilution limit of the functional. The results look very accurate and show three-body interactions much smaller than the pair depletion ones, revealing that these are strongly influenced by correlations and have a decay length similar to the two-body depletion potential. The results are compared with the predictions of the Asakura-Oosawa model for the triplet interactions.

DOI: 10.1103/PhysRevE.64.011403

PACS number(s): 82.70.Dd, 61.20.Gy, 64.75.+g

### I. INTRODUCTION

Asymmetric mixtures composed of species of highly different particle size have wide physical interest, covering the study of colloidal suspensions and macromolecular solutions. In these systems the component of large size, a colloid or a macromolecule, is surrounded by a fluid composed of small particles layered around it. The effective interaction exerted between two or more large particles, is in general given by both the bare interaction acting between them, e.g., of electrostatic nature, and the forces that may be of entropic origin alone, called depletion interactions, arising from the variation of the free energy of the surrounding fluid with the configuration of the larger particles [1]. To lowest order, the depletion effect can be described in terms of the Asakura-Oosawa (AO) theory [2,3] where the fluid is taken as an ideal gas and the effective potential is computed as the variation of the volume available to the fluid with the colloids configuration. According to the simple AO theory, the depletion potential is a monotonic function of the colloids separation.

Depletion interactions arise from the presence of the fluid surrounding large colloids, the larger the difference in size between the two components, the stronger the resulting effective interaction. Moreover, the presence of excluded volume effects and internal correlations of the surrounding fluid, modulates the effective interaction between the large particles in a nontrivial way [4].

Depletion forces are, in principle, many body in nature [5]. For example, when three particles approach each other, the overall depletion interaction is not simply given by the sum of two-body interactions, as seen by computing triplet forces within the AO correlation-free picture. The magnitude of such triplet depletion forces is of interest to understand the nature of solvent-mediated interactions and in designing good two-body parametrization of the effective potential between colloids [5–8]. As for the two-body case, the sum of the interaction due to AO interactions for a given three-particle configuration, and the fluid internal correlations, is expected to give rise to a modulated shape in the triplet depletion forces.

In the present paper we are interested in hard spheres (HS) and in computing the triplet depletion interaction exerted between three large hard spheres surrounded by a solvent composed of small hard spheres. To this purpose, we use density-functional theory (DFT) as the theoretical frame-

work to provide accurate numerical results [9]. A previous calculation has already been presented elsewhere [10] where DFT was employed in the form of the Rosenfeld's "fundamental measure" functional [11]. By minimizing the free energy on a three-dimensional (3D) computational grid at different configurations of the three large HS, the triplet depletion forces were computed by a brute force approach. In general, the numerical implementation used to minimize the Rosenfeld functional in a fully three-dimensional geometry suffers by a serious drawback due to the large amount of grid points needed to accurately solve the computational problem [12]. In fact, the rapid spatial variation of the fluid density for a large size ratio between the two components (such as 5:1) and the intrinsically singular nature of the functional, require a number of grid points that is beyond the actual CPU and memory capabilities. In the previous work, in order to facilitate the calculation, a locally adaptive grid was used to increase the numerical resolution in proximity of the large hard spheres, where the density varies more rapidly [10]. The approach has provided a qualitative, although rough, observation of triplet depletion forces but, when looking at the size of the numerical error bars as compared to the triplet forces, the results were somewhat inconclusive.

In the present paper, we employ an approach different from the previous attempt, by adopting the recent theoretical advances due to Roth *et al.* [8]. Following these authors, we compute the pair and triplet depletion forces by using a refined form of the potential distribution theorem, the so-called infinite dilution limit, in order to reduce the problem of calculating the free energy of three particles to the case of only two particles embedded in the solvent of small HS. By exploiting the cylindrical symmetry of two large HS in the solvent fluid, the problem is reduced from a three-dimensional to a two-dimensional one. Similarly, Roth *et al.* previously computed pair depletion interactions in comparison with Monte Carlo results [13], showing that the method is viable and accurate in DFT. By using the formulation of these authors, we are able to obtain very accurate depletion curves and provide the first quantitative observation of triplet depletion forces.

### II. DFT FOR HARD SPHERES AND THE INFINITE DILUTION LIMIT

We consider  $N_o$  large spheres of diameter  $\sigma_b$  generating an external field for a mixture of small spheres of diameter

$\sigma_s$  and density profile  $\rho_s(\mathbf{r})$ , and large spheres of diameter  $\sigma_b$  and density profile  $\rho_b(\mathbf{r})$ . The size ratio between the two components is  $\alpha = \sigma_b/\sigma_s$ . Given a configuration  $\{\mathbf{R}_i\}$  ( $1 \leq i \leq N_o$ ) of the large spheres, the two densities depend parametrically on  $\{\mathbf{R}_i\}$  and satisfy the constraints

$$\begin{aligned} \rho_s(\mathbf{r}) &= 0, \text{ for } |\mathbf{r} - \mathbf{R}_i| < (\sigma_b + \sigma_s)/2 \\ \rho_b(\mathbf{r}) &= 0, \text{ for } |\mathbf{r} - \mathbf{R}_i| < \sigma_b. \end{aligned} \quad (1)$$

In the grand canonical ensemble, the equilibrium profiles  $\rho_\nu(\mathbf{r})$ ,  $\nu = s, b$ , minimize the grand potential

$$\begin{aligned} \Omega([\rho_s(\mathbf{r}), \rho_b(\mathbf{r})]; \{\mathbf{R}_i\}) &= \mathcal{F}[\rho_s(\mathbf{r}), \rho_b(\mathbf{r})] + \sum_{\nu=s,b} \int \rho_\nu(\mathbf{r}) \\ &\quad \times [V_\nu^{ext}(\mathbf{r}; \{\mathbf{R}_i\}) - \mu_\nu^0] d\mathbf{r}, \end{aligned} \quad (2)$$

where  $V_\nu^{ext}(\mathbf{r}; \{\mathbf{R}_i\})$  is the external potential,  $\mu_\nu^0$  the reservoir chemical potential, and  $\mathcal{F}[\rho_s(\mathbf{r}), \rho_b(\mathbf{r})]$  the Helmholtz free energy, customarily split into ideal and excess parts

$$\mathcal{F}[\rho_s(\mathbf{r}), \rho_b(\mathbf{r})] = \mathcal{F}_{id}[\rho_s(\mathbf{r}), \rho_b(\mathbf{r})] + \mathcal{F}_{ex}[\rho_s(\mathbf{r}), \rho_b(\mathbf{r})], \quad (3)$$

where

$$\mathcal{F}_{id}[\rho_s(\mathbf{r}), \rho_b(\mathbf{r})] = k_B T \sum_{\nu=s,b} \int \rho_\nu(\mathbf{r}) \{ \log[\Lambda_\nu^3 \rho_\nu(\mathbf{r})] - 1 \} d\mathbf{r}. \quad (4)$$

$\Lambda_\nu$  being the de Broglie thermal wavelength of species  $\nu$ .

To date, the most accurate free-energy functional for hard spheres is the Rosenfeld's "fundamental measure" functional [14,11]. Rosenfeld functional for a homogeneous fluid turns into the Percus-Yevick compressibility equation of state [15], with a wide range of validity versus the packing fraction. Among several different forms of the functional proposed in the literature [16], we have chosen the one that correctly provides freezing of the one-component hard-sphere system, with the proper treatment of the zero-dimensional limit of the functional. Recently, Roth and Dietrich have successfully tested the reliability of the Rosenfeld functional for binary mixtures close to a planar hard wall [18], while we have tested the functional for ternary mixtures of HS in confined geometries [17,19] with Monte Carlo results.

The Rosenfeld functional for HS has the form

$$\begin{aligned} \mathcal{F}_{ex}[\rho_s(\mathbf{r}), \rho_b(\mathbf{r})] &= k_B T \int \Phi(n_\alpha(\mathbf{r})) d\mathbf{r} \\ &= k_B T \int \left\{ -n_0(\mathbf{r}) \log[1 - n_3(\mathbf{r})] \right. \\ &\quad + \frac{n_1(\mathbf{r})n_2(\mathbf{r}) - \mathbf{n}_{V1}(\mathbf{r}) \cdot \mathbf{n}_{V2}(\mathbf{r})}{1 - n_3(\mathbf{r})} \\ &\quad \left. + \frac{[n_2(\mathbf{r})(1 - \xi(\mathbf{r})^2)]^3}{24\pi[1 - n_3(\mathbf{r})]^2} \right\} d\mathbf{r}, \end{aligned} \quad (5)$$

with the following weighted densities defined as

$$\begin{aligned} n_0(\mathbf{r}) &= \sum_\nu \frac{1}{4\pi\sigma_\nu^2} \int \rho_\nu(\mathbf{r}') \delta(|\mathbf{r} - \mathbf{r}'| - \sigma_\nu) d\mathbf{r}' \\ &= \sum_\nu \frac{1}{4\pi\sigma_\nu^2} n_{2,\nu}(\mathbf{r}), \end{aligned}$$

$$\begin{aligned} n_1(\mathbf{r}) &= \sum_\nu \frac{1}{4\pi\sigma_\nu} \int \rho_\nu(\mathbf{r}') \delta(|\mathbf{r} - \mathbf{r}'| - \sigma_\nu) d\mathbf{r}' \\ &= \sum_\nu \frac{1}{4\pi\sigma_\nu} n_{2,\nu}(\mathbf{r}), \end{aligned}$$

$$n_2(\mathbf{r}) = \sum_\nu \int \rho_\nu(\mathbf{r}') \delta(|\mathbf{r} - \mathbf{r}'| - \sigma_\nu) d\mathbf{r}' = \sum_\nu n_{2,\nu}(\mathbf{r}),$$

$$n_3(\mathbf{r}) = \sum_\nu \int \rho_\nu(\mathbf{r}') \theta(|\mathbf{r} - \mathbf{r}'| - \sigma_\nu) d\mathbf{r}' = \sum_\nu n_{3,\nu}(\mathbf{r}),$$

$$\begin{aligned} \mathbf{n}_{V1}(\mathbf{r}) &= \sum_\nu \frac{1}{4\pi\sigma_\nu} \nabla_{\mathbf{r}} \int \rho_\nu(\mathbf{r}') \theta(|\mathbf{r} - \mathbf{r}'| - \sigma_\nu) d\mathbf{r}' \\ &= \nabla_{\mathbf{r}} \sum_\nu \frac{1}{4\pi\sigma_\nu} n_{3,\nu}(\mathbf{r}), \end{aligned}$$

$$\mathbf{n}_{V2}(\mathbf{r}) = \sum_\nu \nabla_{\mathbf{r}} \int \rho_\nu(\mathbf{r}') \theta(|\mathbf{r} - \mathbf{r}'| - \sigma_\nu) d\mathbf{r}' = \nabla_{\mathbf{r}} \sum_\nu n_{3,\nu}(\mathbf{r}), \quad (6)$$

where we have introduced the partial weighted densities

$$\begin{aligned} n_{2,\nu}(\mathbf{r}) &= \int \rho_\nu(\mathbf{r}') \delta(|\mathbf{r} - \mathbf{r}'| - \sigma_\nu) d\mathbf{r}', \\ d\mathbf{r}' n_{3,\nu}(\mathbf{r}) &= \int \rho_\nu(\mathbf{r}') \theta(|\mathbf{r} - \mathbf{r}'| - \sigma_\nu), \end{aligned} \quad (7)$$

and the function  $\xi(\mathbf{r}) = |\mathbf{n}_{V2}|/n_2(\mathbf{r})$ .

In general, the weighted densities can be rewritten in terms of scalar and vectorial weight functions  $\omega_{\alpha,\nu}$ , via the equation

$$n_{\alpha,\nu} = \int \rho_\nu(\mathbf{r}') \omega_{\alpha,\nu}(\mathbf{r} - \mathbf{r}') d\mathbf{r}'. \quad (8)$$

By functional differentiation of the total free energy, the equilibrium densities are found to satisfy the following self-consistent equation

$$\rho_\nu(\mathbf{r}) = \rho_\nu^0 \exp[-\beta V_\nu^{ext}(\mathbf{r}) + c_\nu^{(1)}(\mathbf{r})], \quad (9)$$

where  $\rho_\nu^0 = \Lambda_\nu^{-3} \exp(\beta\mu_\nu)$  is the reservoir bulk density and

$$c_\nu^{(1)}(\mathbf{r}) = -\beta \frac{\delta \mathcal{F}^{ex}}{\delta \rho_\nu(\mathbf{r})} \quad (10)$$

is the one-body direct pair-correlation function.

The depletion potential between two large HS embedded in a sea of small HS, is defined as the difference in grand potential between two configurations in which the pair is at distance  $R_{12}$  and at infinity, respectively:

$$W_2(R_{12}) = \Omega([\rho_s(\mathbf{r}), \rho_b(\mathbf{r})]; R_{12}) - \Omega([\rho_s(\mathbf{r}), \rho_b(\mathbf{r})]; R_{12} \rightarrow \infty). \quad (11)$$

Roth *et al.* have shown that computing the depletion potential can be greatly simplified by writing the depletion potential in terms of the one-body direct correlation function of the large spheres

$$W_2(R_{12}) = c_b^{(1)}(R_{12} \rightarrow \infty) - c_b^{(1)}(R_{12}). \quad (12)$$

The previous expression can be applied once an explicit form of the excess free energy is provided, as for the Rosenfeld free energy functional. In this case,

$$c_b^{(1)}(\mathbf{r}) = - \int \sum_\alpha A_\alpha(\mathbf{r}') \omega_{b,\alpha}(\mathbf{r} - \mathbf{r}') d\mathbf{r}', \quad (13)$$

where we have defined

$$A_\alpha(\mathbf{r}) = \frac{\partial \Phi}{\partial n_\alpha}(\mathbf{r}). \quad (14)$$

If we set the density of the large HS to zero, i.e., in the infinite dilution limit of this species being unperturbed, the weighted densities take the form:

$$n_\alpha(\mathbf{r}) = \int \rho_s(\mathbf{r}') w_{s,\alpha}(\mathbf{r} - \mathbf{r}') d\mathbf{r}'. \quad (15)$$

Equation (13) provides the so-called direct limit route to compute  $W(r)$ . In fact, given the small spheres density that minimizes the Rosenfeld functional, the weighted densities  $n_\alpha$  and the function  $A_\alpha$  can be evaluated to yield the pair depletion potential (12).

Alternatively, a numerical procedure can be applied to take the infinite dilution limit. This is obtained by considering the Rosenfeld free energy as a functional of both the small and large HS densities. The large HS density is taken small enough to leave the small HS density unperturbed, and the depletion potential is obtained as

$$W(R_{12}) = -k_B T \lim_{\rho_b \rightarrow 0} \ln \frac{\rho_b(R_{12})}{\rho_b(R_{12} \rightarrow \infty)}. \quad (16)$$

The two distinct procedures allow to compute the pair depletion potential by considering the external potential of a single large HS surrounded by a sea of small particles, eventually together with an infinitesimal density of the large spheres if the numerical limit is used. In both cases, the computation is

simplified by exploiting the symmetry of the external potential, in fact reducing the problem to a one-dimensional calculation.

An analogous procedure can be applied to compute the triplet depletion potential of three large HS embedded in the sea of small HS. The triplet depletion potential is equal to the difference in grand potential between a configuration in which three particles have overlapping excluded volume and a configuration when the three particles have separations so large that they do not see each other (i.e., the correlations induced by each sphere on the surrounding fluid are mutually independent):

$$W_3(\mathbf{R}_1, \mathbf{R}_2, \mathbf{R}_3) = \Omega(\mathbf{R}_1, \mathbf{R}_2, \mathbf{R}_3) - \Omega(\mathbf{R}_1, \mathbf{R}_2 \rightarrow \infty, \mathbf{R}_3 \rightarrow \infty) - \Omega(\mathbf{R}_1 \rightarrow \infty, \mathbf{R}_2, \mathbf{R}_3 \rightarrow \infty) - \Omega(\mathbf{R}_1 \rightarrow \infty, \mathbf{R}_2 \rightarrow \infty, \mathbf{R}_3) \quad (17)$$

where we have dropped the functional dependence on densities for simplicity. The three-body correction to the depletion interaction is therefore taken to be

$$\Delta W_3(\mathbf{R}_1, \mathbf{R}_2, \mathbf{R}_3) = W_3(\mathbf{R}_1, \mathbf{R}_2, \mathbf{R}_3) - W_2(R_{12}) - W_2(R_{13}) - W_2(R_{23}), \quad (18)$$

where  $W_2$  for different two-body configurations is computed via independent calculations.

We remark that the infinite dilution limit is applicable to compute triplet depletion interactions via both computer simulations and experiments. Given the pair depletion interaction, an accurate expression for the free-energy functional is needed to construct the triplet interactions.

We now evaluate the triplet contribution to the depletion potential within the AO model that, as we will show, arises from the triply excluded volume of three spheres surrounded by a perfect gas. Let us consider a system made of three particles, embedded in a fluid at constant density  $\rho_s^0$  and contained in a region of volume  $V_T$ . Each sphere determines a region precluded to density of volume  $V = \pi(\sigma_b + \sigma_s)^3/6$ . Now, let us consider the volume doubly precluded to the density and formed by a pair  $i, j$  of overlapping spheres  $V_{ij}$  and the volume triply precluded to the density and formed by a triplet  $i, j, k$  of particles,  $V_{ijk}$ . A simple geometrical argument shows that, given three overlapping spheres, the volume available to the surrounding fluid is:

$$V_{123}^{av} = V_T - 3V + V_{12} + V_{13} + V_{23} - V_{123}. \quad (19)$$

Similarly,  $V_{ij}^{av} = V_T - 2V + V_{ij}$  is the available volume due to two overlapping spheres.

The AO pair depletion potential is given by

$$\begin{aligned} W_2^{AO} &= -k_B T \rho_s^0 [V_{ij}^{av} - (V_T - 2V)] \\ &= -k_B T \rho_s^0 [V_T - 2V + V_{ij} - V_T + 2V] \\ &= -k_B T \rho_s^0 V_{ij}, \end{aligned} \quad (20)$$

where we have dropped the dependence on the sphere positions for clarity. Analogously, the three-body depletion potential is

$$\begin{aligned} W_3^{\text{AO}} &= -k_B T \rho_s^0 [V_{123}^{av} - (V_T - 3V)] \\ &= -k_B T \rho_s^0 [V_T - 3V + V_{12} + V_{13} + V_{23} - V_{123} - V_T + 3V] \\ &= -k_B T \rho_s^0 [V_{12} + V_{13} + V_{23} - V_{123}], \end{aligned} \quad (21)$$

where the pair and triplet depletion potentials are both negative and do not depend on the volume of the singly excluded regions. The corresponding three-body correction is derived from Eq. (18), yielding:

$$\Delta W_3^{\text{AO}} = k_B T \rho_s^0 V_{123}, \quad (22)$$

which is a positive quantity, depending on the triply excluded volume only, and monotonic as the three spheres move away from each other.

Before concluding this section, we remark that  $c^{(1)}(\mathbf{r})$  needs to be computed by either using the direct limit of the Rosenfeld functional or the numerical limit, analogously to Eq. (16), and in both cases the Rosenfeld functional needs to be minimized given a configuration of two large HS. The cylindrical symmetry can be fully exploited to increase the accuracy of the calculation with respect to a brute force approach where, in the presence of three large HS, the calculation involves a fully three dimensional minimization of the functional. Moreover, instead of obtaining few points of the depletion potential, the method allows us to study the whole three-body potential surface for a given two spheres separation.

We finally note that Eq. (13) proves computationally more convenient than the numerical limit route, since for the former, only the one-component form of the functional needs to be minimized. Moreover, the performances are also different, since the numerical limit route implies an extra computational cost due to the use of the large sphere density and further iterations in the free-energy minimization are required. Therefore, we will present numerical results obtained via the direct limit of the functional to compute pair and triplet depletion interactions.

### III. NUMERICAL IMPLEMENTATION

To solve the Rosenfeld functional for a pair of large HS the optimal choice is to use cylindrical coordinates. As discussed in the previous section, we consider here only the density field of the small spheres  $\rho_s(\mathbf{r})$ , and first look at the scalar weight functions  $\omega_{2,s}$  and  $\omega_{3,s}$ . The relative weighted densities are expressed in cylindrical coordinates as

$$\begin{aligned} n_{\alpha,s}(\mathbf{r}) &= \int d\mathbf{r}' \rho_s(\mathbf{r}') \omega_{\alpha,s}(|\mathbf{r} - \mathbf{r}'|) \\ &= \int_{-\infty}^{\infty} dz' \int_0^{\infty} dr' 2\pi r' \rho_s(r', z') g_{\alpha,s}(r, r', z - z'), \end{aligned} \quad (23)$$

where

$$g_{\alpha,s}(r, r', z - z') = \frac{1}{2\pi} \int_0^{2\pi} d\phi \omega_{\alpha,s}[f(r, r', z - z')], \quad (24)$$

and

$$\begin{aligned} f(r, r', z - z') &= |\mathbf{r} - \mathbf{r}'| - \frac{\sigma_s}{2} \\ &= [r^2 + r'^2 - 2rr' \cos \phi \\ &\quad + (z - z')^2]^{1/2} - \frac{\sigma_s}{2}. \end{aligned} \quad (25)$$

If we transform the angular integral from the variable  $\phi$  into the variable  $f$ , we have

$$\begin{aligned} d\phi &= \frac{4(f + \sigma_s/2)}{\{4r^2 r'^2 - [c^2 - (f + \sigma_s/2)^2]^2\}^{1/2}} df, \\ \cos \phi &= \frac{[c^2 - (f + \sigma_s/2)^2]^2}{2rr'}, \end{aligned} \quad (26)$$

where we have introduced the function  $c(r, r', z - z')$  being

$$c^2 = r^2 + r'^2 + (z - z')^2. \quad (27)$$

We note that in expression (26) for the differential  $d\phi$  a factor 2 needs to be introduced given the two possible solutions for  $\cos \phi$  in the range  $(0 \leq \phi \leq 2\pi)$ .

The explicit calculation of  $n_2(r, z)$  then yields

$$\begin{aligned} n_2(r, z) &= \int dr' \int dz' \int df \\ &\quad \times \frac{4r'(f + \sigma_s/2) \delta(f)}{\{4r^2 r'^2 - [c^2 - (f + \sigma_s/2)^2]^2\}^{1/2}} \rho_s(r', z') \\ &= \int_{\max(r - \sigma_s/2, 0)}^{r + \sigma_s/2} dr' \left\{ \int_{e_1}^{e_2} dz' \right. \\ &\quad \left. + \int_{-e_2}^{-e_1} dz' \right\} \frac{2r' \sigma_s \rho_s(r', z')}{[4r^2 r'^2 - (c^2 - \sigma_s^2/4)^2]^{1/2}}, \end{aligned} \quad (28)$$

where the extrema of integration are defined as

$$\begin{aligned} e_1 &= \max([\sigma_s^2/4 - (r' + r)^2]^{1/2} + z, z), \\ e_2 &= \min([\sigma_s^2/4 - (r' - r)^2]^{1/2} + z, z + \sigma_s/2), \end{aligned} \quad (29)$$

and provided that  $e_1 \leq e_2$ .

The explicit calculation of  $n_3(r, z)$  proceeds similarly by applying the same transformation in the angular variable. The resulting expression is

$$\begin{aligned}
 n_3(r, z) &= \int dr' \int dz' \int df \frac{4r'(f + \sigma_s/2)\theta(f)}{\{4r^2r'^2 - [c^2 - (f + \sigma_s/2)^2]\}^{1/2}} \rho_s(r', z') \\
 &= \int dr' \int dz' \int_{\max(-\sigma_s/2, -[\sigma_s^2/4 - (r' + r)^2 - (z - z')^2]^{1/2})}^{\min(0, -[\sigma_s^2/4 - (r' - r)^2 - (z - z')^2]^{1/2})} df \frac{4r'(f + \sigma_s/2)}{\{4r^2r'^2 - [c^2 - (f + \sigma_s/2)^2]\}^{1/2}} \rho_s(r', z') \\
 &= \int_{\max(r - \sigma_s/2, 0)}^{r + \sigma_s/2} dr' \left\{ \int_0^{e_3} dz' + \int_{e_4}^{e_5} dz' \right\} \left\{ \pi - 2 \tan^{-1} \left[ \frac{c^2 - \sigma_s^2/4}{[4r^2r'^2 - (c^2 - \sigma_s^2/4)^2]^{1/2}} \right] \right\} 2\pi \rho_s(r', z'), \quad (30)
 \end{aligned}$$

where the extrema of integration are

$$\begin{aligned}
 e_3 &= \max\{[\sigma_s^2/4 - (r + r')^2]^{1/2}, 0\}, \\
 e_4 &= \min\{\sigma_s/2 + z, [\sigma_s^2/4 - (r - r')^2]^{1/2} + z\}, \\
 e_5 &= \max\{[\sigma_s^2/4 - (r + r')^2]^{1/2} + z, z\}. \quad (31)
 \end{aligned}$$

Similar lengthy expressions can be obtained for the vector weighted density. However, a more convenient form for numerical purposes is obtained by using the relation  $n_{V2}(\mathbf{r}) = \nabla_{\mathbf{r}} n_3(\mathbf{r})$ , so that the vector weighted densities can be computed by numerical differentiation of the scalar weighted density  $n_3(\mathbf{r})$ .

Due to the dependence of the weighted densities on  $(z - z')$  only, the integrals in the  $z$  direction are easily computed in Fourier space by using the convolution theorem, therefore, with a performance that scales linearly with the number of grid points in the axial direction. Vice versa, in the radial direction, the integrals are not convolutions any more. These need to be computed with a cost that scales with the number of grid points per hard-sphere times the number of grid points in the radial direction.

A particular care is needed in computing the radial integrals. In fact, spurious numerical correlations arise due to the discrete computational grid that is unable to account for the fast variation of the weight functions close to the origin. For instance, this can be observed by direct inspection of  $\omega_{2,s}(r, r')$ , the weight function with the strongest spatial variation, versus  $r'$ . The singular behavior is particularly relevant as  $r \rightarrow 0$ .

To alleviate this problem, we have reformulated the minimization procedure by considering only quantities as differences from the corresponding bulk values, which can be computed analytically, their corresponding values given by the Percus-Yevick equation of state. We define the following quantities:

$$\begin{aligned}
 \Delta n_{\alpha}(\mathbf{r}) &= \int (\rho_s(\mathbf{r}') - \rho_s^0) \omega_{v,s}(\mathbf{r} - \mathbf{r}') d\mathbf{r}', \\
 \Delta A_{\alpha}(\mathbf{r}) &= A_{\alpha}(\mathbf{r}) - A_{\alpha}^0 = \frac{\partial \Phi}{\partial n_{\alpha}}(\mathbf{r}) - A_{\alpha}^0, \quad (32)
 \end{aligned}$$

where  $n_{\alpha}(\mathbf{r}) = \Delta n_{\alpha}(\mathbf{r}) + n_{\alpha}^0$ , and  $n_{\alpha}^0$  is the bulk value of the weighted density, known analytically. Similarly,  $A_{\alpha}(\mathbf{r})$  is de-

finied by Eq. (14), and its bulk value  $A_{\alpha}^0$  is known analytically. Therefore, the self-consistent Eq. (9) can be solved by computing at each iteration step

$$c_s^{(1)}(\mathbf{r}) = - \sum_{\alpha} \int \Delta A_{\alpha}(\mathbf{r}') \omega_{\alpha,s}(\mathbf{r}' - \mathbf{r}) d\mathbf{r}'. \quad (33)$$

The advantage of this formulation relies in that, since the quantities  $\Delta \rho_s$ ,  $\Delta n_{\alpha}$ , and  $\Delta A_{\alpha}$  are zero in the bulk, their spatial variations are reduced with respect to their absolute values. Moreover, wherever a region precluded to density is present in the computational domain, such as inside a large hard sphere, the local values of  $n_{\alpha}$  and  $A_{\alpha}$  are taken to be equal to their bulk values.

#### IV. RESULTS

As a preliminary benchmark of the described method, we have computed the depletion potential of a pair of large hard

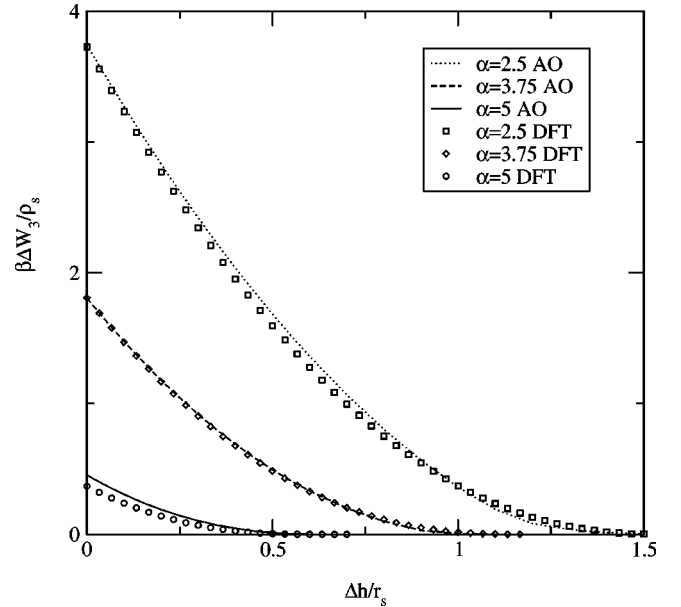


FIG. 1. The three-body correction to the potential,  $\Delta W_3 / \rho_0 k_B T$ , when a third sphere is moved a height  $\Delta h$  away from two spheres at contact for size ratio  $\alpha = 2.5, 3.75$ , and  $5$ . The full lines are from the AO model and the symbols are the numerical DFT results in the infinite dilution limit (with a packing fraction of small spheres of  $\pi/30\,000$ ).

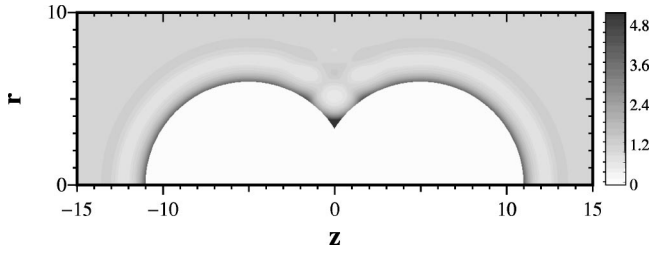


FIG. 2. Contour plot of the density of small spheres around two large spheres. The separation of the large spheres is 10 in units of the small sphere radius  $r_s$ . The  $z$  coordinate is along the line of the centers of the large spheres and the  $r$  coordinate is perpendicular to this. The density values are measured in dimensionless units of  $\rho(\mathbf{r})/\rho_s$ , where  $\rho_s$  is the bulk small hard-sphere density of 0.075. The size ratio of the small spheres to large spheres is  $\alpha=5$ , and the packing fraction is  $\eta=\pi/10$ . The cell size is  $60r_s$  in the  $z$  direction (along the line of the centers of the large spheres) and  $20r_s$  along the  $r$  direction in cylindrical coordinates. The grid used is made of  $1800 \times 600$  points.

spheres for three different values of the packing fraction of the surrounding fluid,  $\eta=\rho_s\sigma_s^3\pi/6$ , and for a size ratio  $\alpha=5$  in cylindrical coordinates (2D) and via the infinite dilution limit in spherical coordinates (1D) (see Fig. 7 of Ref. [20]). A similar test has been previously made [8] for the size ratio  $\alpha=10$ , by comparing the Rosenfeld functional results versus molecular dynamics data [13]. We have obtained nearly perfect agreement between the 1D and 2D approaches, proving the quality of the performances of the Rosenfeld functional via a self-consistent test. At the same time, the numerical procedure in cylindrical coordinates looks accurate, lending confidence on the solution of the three-body problem via the infinite dilution route.

As a different preliminary test, we have considered the three-body correction to the depletion potential  $\Delta W_3$  obtained via the infinite dilution route and the Asakura-Oosawa prediction, the latter becoming exact in the limit of a small packing fraction of the surrounding fluid. The AO depletion potential is obtained by using Eq. (22) and where the overlap volume of three large HS has been computed via a numerical integration procedure.

Figure 1 shows  $\Delta W_3$  for three spheres in isosceles geometry, with two spheres forming the base at contact and the third sphere displaced vertically at height  $\Delta h$ . The calculation is repeated for three different values of  $\eta$ . In all cases, good agreement is found between the two approaches, in particular for an intermediate value of the size ratio. A simple but tedious geometrical argument shows that for larger size ratio, the AO three-body depletion potential drops to zero when the vertical separation exceeds [21]

$$\Delta h_{max} = \frac{1}{2} [\sqrt{2\sigma_s\sigma_b + \sigma_s^2} - (1 - \sqrt{3})\sigma_b + \sigma_s]. \quad (34)$$

Moreover, as the size ratio is increased, the interaction becomes more short ranged and disappears continuously when  $\alpha > 6.46$ .

The DFT approach allows us to inspect directly the local behavior of the density, as illustrated in Fig. 2, where we

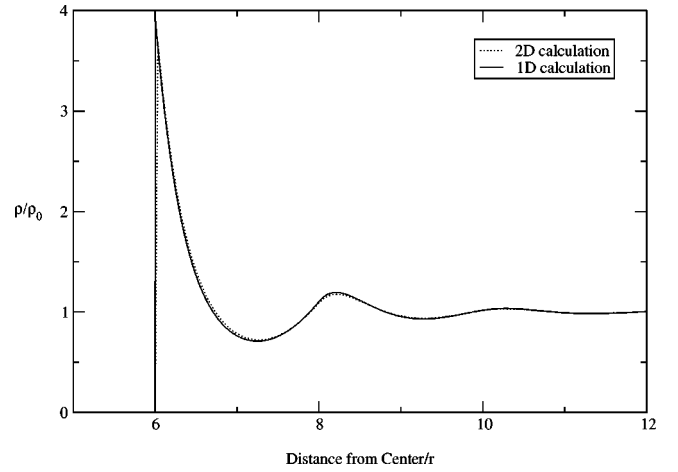


FIG. 3. Comparison of density profiles of small spheres around a single large sphere from the 1D and 2D approaches for a system with  $\alpha=5$  and  $\eta=\pi/10$ .  $R$  is the distance from the center of the sphere in  $r_s$  units. The 1D spherically symmetric calculation uses 327 radial grid points per small sphere radius and the 2D cylindrically symmetric code uses 30 grid points per small sphere radius.

report the contour plot of the density around a pair of spheres at contact. The density exhibits maxima close to the HS borders, and in particular close to the contact point between the two spheres. The contour plot refers to a size ratio  $\alpha=5$  and a packing fraction  $\eta=\pi/10$ . The density map has been computed for a cylindrical simulation cell size of  $30\sigma_s$  in the axial direction, and  $10\sigma_s$  in the radial direction. The computational grid is composed of  $1800 \times 600$  points in the two directions, respectively.

The numerical accuracy of the spherical versus cylindrical grid methods has been compared in Fig. 3, where we report

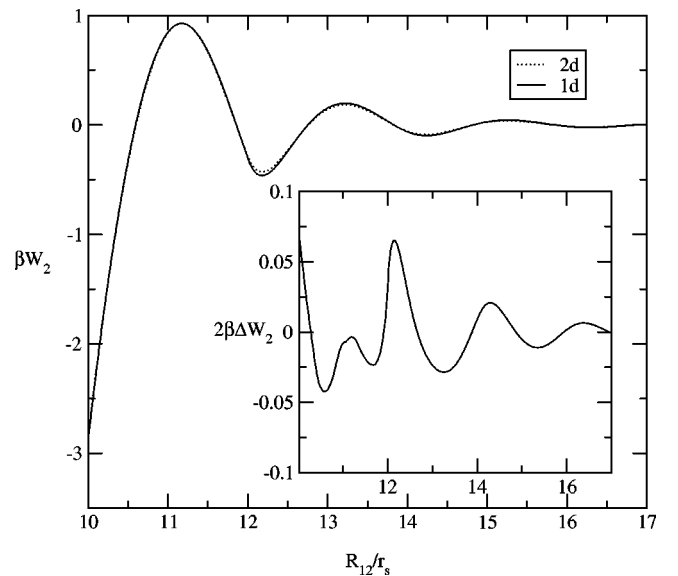


FIG. 4. The two-body depletion potential  $W_2$  from both the 1D and 2D calculations, for  $\alpha=5$  and  $\eta=\pi/10$ . The inset graph shows twice the difference for these potentials. The 1D spherically symmetric calculation uses 327 radial grid points per small sphere radius and the 2D cylindrically symmetric calculation uses 30 grid points per small sphere radius.

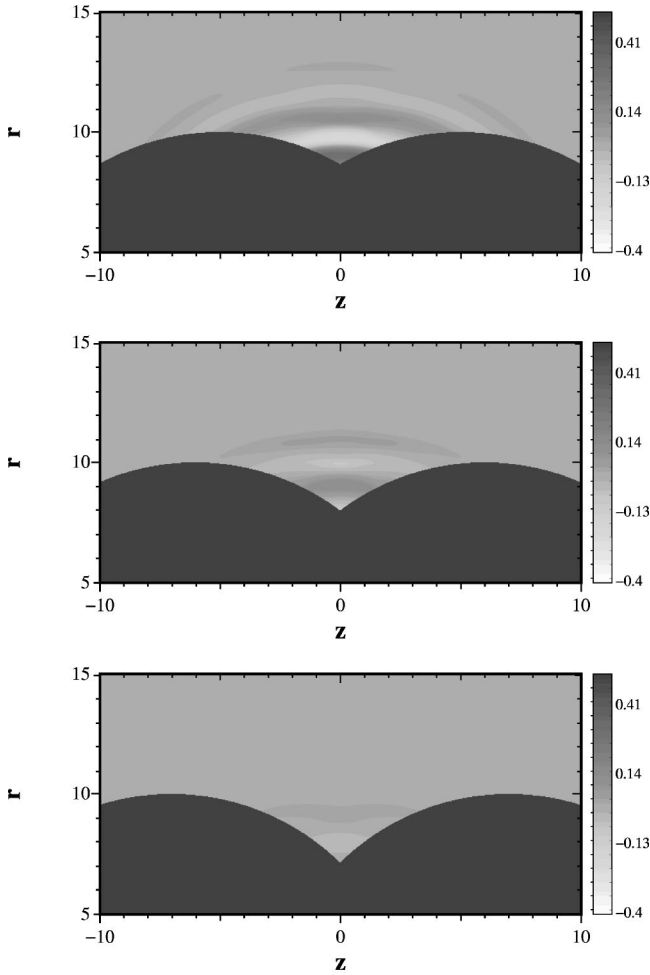


FIG. 5. Contour plot of the three-body contribution  $\Delta W_3$  felt by a third large hard sphere near two other spheres that are separated by  $R_{12} = 10 r_s$  (upper panel),  $12 r_s$  (middle panel), and  $14 r_s$  (lower panel). The packing fraction of the small spheres is  $\eta = \pi/10$ . Outside the region, there is no observable three-body potential and the white areas indicate the regions inaccessible to the third hard sphere. The gray scale indicated is in  $k_B T$  units.  $r$  is the radial coordinate, and  $z$  is the distance along the axis, both in  $r_s$  units.

the density profile of small spheres around a single large sphere, obtained via the 1D and 2D methods. For this test, the size ratio is  $\alpha = 5$  and the packing fraction is  $\eta = \pi/10$ . In the 1D calculation, we used 327 grid points per small sphere radius, whereas for the 2D calculation we used 30 grid points per small sphere radius. The contact values of the density are found to be  $3.92 \rho_s$  and  $3.96 \rho_s$  for the 1D and 2D methods, respectively. The discrepancy of around 1% will reflect on the depletion forces, since these are surface integrals of the density of the small spheres at contact with the large spheres [22,5]. Overall, the two profiles show excellent matching at all distances from the large sphere, so that with the chosen grid resolution, we can proceed in computing three-body depletion potentials.

The numerical error present in our calculations has been estimated by considering the pair depletion potential  $W_2$  obtained with the 2D and 1D distinct calculations, and shown in Fig. 4. The difference between the two approaches can be

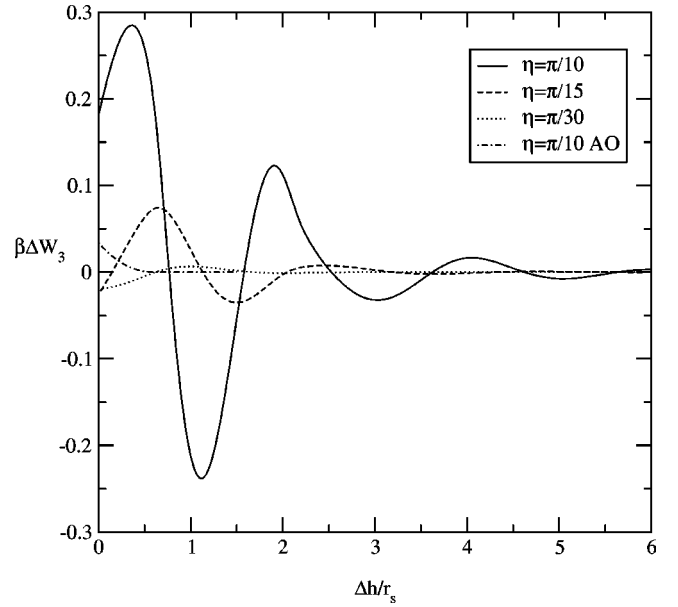


FIG. 6. Plots of the three-body contribution to the depletion potential felt by a third sphere a vertical distance  $\Delta h$  above the contact point with the bottom two spheres. The size ratio is  $\alpha = 5$  and the packing fraction is  $\eta = \pi/10$  (solid curve),  $\pi/15$  (dashed curve), and  $\pi/30$  (dotted curve). The dotted-dashed curve refers to the AO result for  $\eta = \pi/10$ .

considered as a combination of the numerical error due to different grid resolutions and the usage of the approximate Rosenfeld functional. The error is visible in the inset and exhibits limited oscillations smaller than  $0.05 k_B T$  and without a definite trend versus the HS spacing; this error can be considered to be valid also for the three-body depletion potentials reported in the following of the section.

The three-body potentials are computed once the free energy is minimized for the two spheres configuration. In Fig. 5, we report the contour plots of the quantity  $\Delta W_3$  obtained for three different separations of two spheres, for  $\eta = \pi/10$  and  $\alpha = 5$ . The plots show that the three-body potential is highly localized around the center line ( $z = 0$ ) and is at least one order of magnitude smaller than the typical two-body potentials at the same packing fraction. Also, the three-body contribution rapidly disappears when the particle separation becomes larger than  $7 \sigma_s$ . An interesting feature of the contour plots is the circular band structure observed when the large spheres are close to contact.

The behavior of  $\Delta W_3$  is next extracted from the data, considering a three-body isosceles geometry and by using Eq. (18) with  $\mathbf{R}_1 = (-R_{12}/2, 0, 0)$ ,  $\mathbf{R}_2 = (R_{12}/2, 0, 0)$  and  $\mathbf{R}_3 = (0, 0, z)$ , for different values of  $z$ . Figure 6 illustrates  $\Delta W_3$  for  $\alpha = 5$  and at three different packing fractions. The interesting feature of the data is that the three-body potential is highly modulated by correlations as compared to the AO result, also shown in Fig. 6 for  $\eta = \pi/10$ . The AO curve is rather short ranged and is an order of magnitude smaller than the three-body contribution, in contrast to the two-body case where the AO potential has magnitude comparable to the true depletion potential.

The AO three-body contact potential is further analyzed

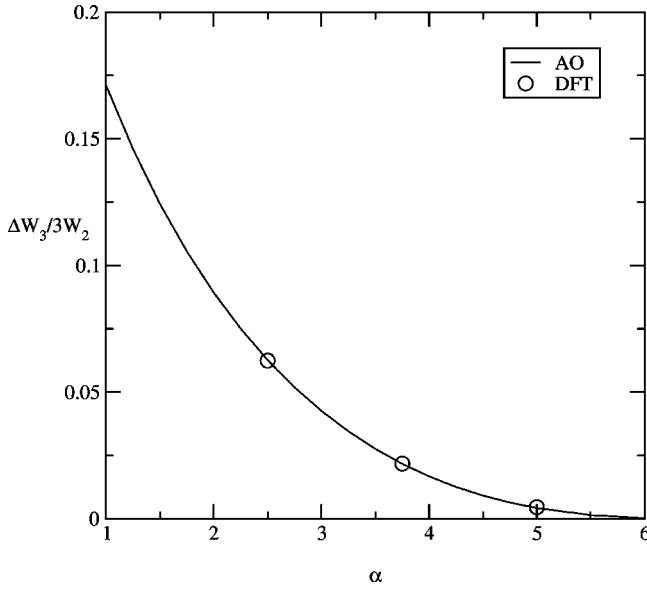


FIG. 7. Plot of the ratio of the three-body potential  $\Delta W_3$  to the pairwise contribution ( $3W_2$ ) when three spheres are at contact versus the size ratio  $\alpha$ , for a packing fraction of  $\eta = \pi/30\,000$ . Full line is for the AO model symbols are the DFT results.

by considering the case of three spheres in contact ( $R_{12} = R_{13} = R_{23} = \sigma_b$ ), and by plotting the ratio  $\Delta W_3/3W_2$ , as in Fig. 7, where the Rosenfeld and the AO results are compared versus the size ratio for a packing fraction of the surrounding fluid of  $\eta = \pi/30\,000$ . The AO and low-density limit of the Rosenfeld functional agree, as expected, and the curve decays quickly at large size ratio and exhibit larger contributions of the three-body terms for smaller size ratios.

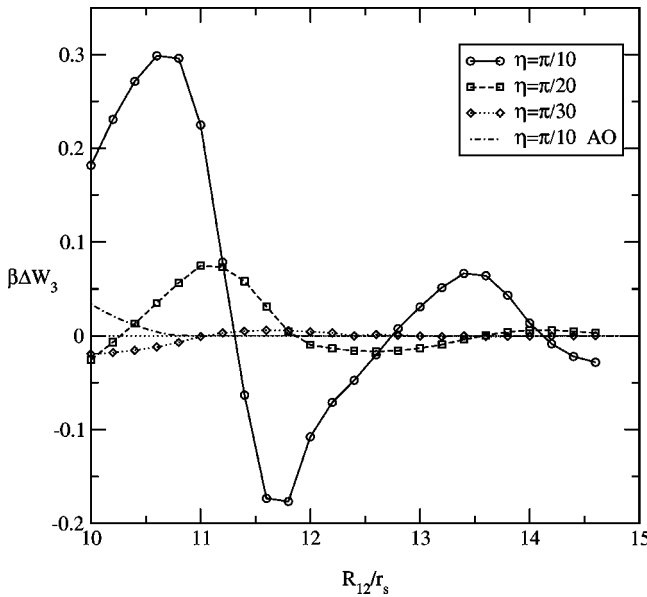


FIG. 8. Plot of the three-body contribution to the depletion potential felt by a third sphere in contact with two spheres separated by a distance  $R_{12}$  in  $r_s$  units, for  $\alpha=5$  and for packing fraction of  $\eta = \pi/10$  (circles),  $\pi/20$  (squares), and  $\pi/30$  (diamonds). The AO result for  $\eta = \pi/10$  is also reported for comparison (dot-dashed line).

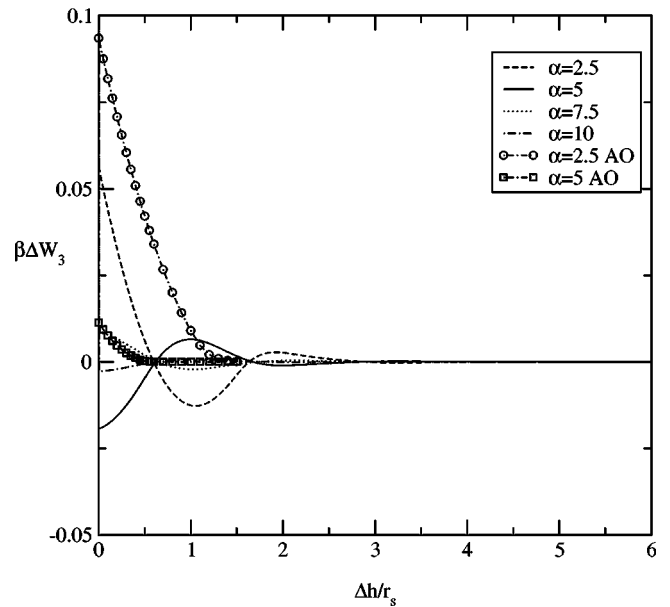
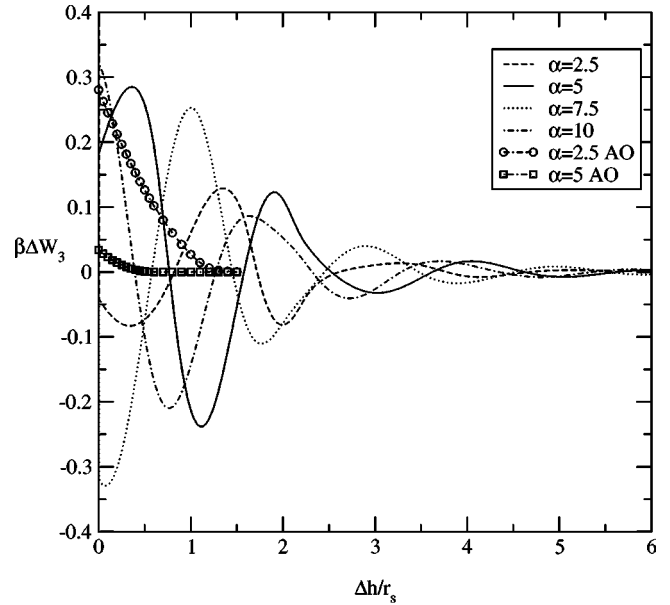


FIG. 9. Plots of the three-body contribution to the depletion potential felt by a third sphere a vertical distance  $\Delta h$  above the contact point with the bottom two spheres, which are in contact. The size ratio of the large to small spheres is given in the legend and AO indicated the Asakura-Oosawa for that size ratio. The top graph is for a packing fraction of the small spheres of  $\pi/10$ , and the bottom graph is for a packing fraction  $\pi/30$ .

Another interesting configuration to analyze the three-body contact forces is when the third sphere is in contact with the bottom spheres, the latter being at variable separation  $R_{12}$ . As Fig. 8 shows, in this case, the correlational oscillations are relatively large and rather different from the AO estimate.

Finally, we have studied the three-body contribution to depletion versus the size ratio, in the same isosceles geometry where the base spheres are in contact and the third sphere is displaced vertically. Figure 9 illustrates the three-body potential for  $\eta = \pi/10$  and  $\eta = \pi/30$ . At the higher

packing fraction of  $\pi/10$ , the magnitude of the three-body potential seems to be relatively unchanged by the size ratio. However, since the strength of the pair interaction is approximately proportional to the size ratio (i.e., increases with large sphere radius), the three-body potential becomes relatively less important as the size ratio is increased. The AO depletion potential seems to have an effect at size ratio  $\alpha = 2.5$ , where it appears to push up the value of the three-body potential. At the lower packing fraction  $\eta = \pi/30$ , the potentials are greatly reduced, but again, the AO potential seems to have an effect for  $\alpha = 2.5$ . This time, however, the effect is quite visible, with the potential initially following the same gradient as the AO potential.

## V. CONCLUSIONS

We have presented a numerical method for computing three-body interactions in hard sphere mixtures within the framework of density-functional theory. The computational effort is greatly reduced by considering the so-called infinite dilution limit of the functional, since the original three-dimensional problem is reconducted to a two-dimensional one. Therefore, by minimizing the free energy in cylindrical coordinates we have obtained a whole family of depletion curves versus the size ratio and the packing fraction.

The obtained results have shown that the three-body interactions are much smaller than the pair depletion ones and are mostly correlation-driven, exhibiting both attractive and repulsive behavior. Since depletion forces can be written as surface integrals of the small sphere density at contact with

the large hard spheres [22,10], the presence of the third sphere induces a surplus or deficit of density at contact, and therefore a modulation of the local kinetic pressure due to the surrounding fluid [5].

Moreover, the triplet contribution to depletion rapidly decays to zero as a third sphere moves away from two spheres with a decay length similar to the corresponding two-body depletion potential. This effect is evident at small packing fraction and the decay is slightly slower as the packing fraction approaches one. We have compared our results with the Asakura-Oosawa correlation-free model, and observed that, although the AO model captures the magnitude of the triplet interactions, only at small packing fraction and small size ratio can the AO picture can be taken as a good estimate for the three-body correction to the depletion interactions. Finally, our results suggest that a similar behavior has to be expected for higher order contributions to depletion interactions. Since the  $n$ th-order AO contribution to depletion potential depends on the overlapping excluded volume of  $n$  large spheres, the  $n$ th-order depletion potential will presumably be smaller by one order of magnitude than the term at lower order.

## ACKNOWLEDGMENTS

The authors wish to thank J. -P. Hansen for his continuous help during the development of this project. Fruitful discussions with R. Evans and R. Roth are kindly acknowledged. D. Goulding thanks the EPSRC for their support and S. Melchionna acknowledges the support of the Leverhulme Trust.

- 
- [1] E. J. W. Verwey and J. T. G. Overbeek, *Theory of the Stability of Lyophobic Colloids* (Elsevier, Amsterdam, 1948). For a recent review, see J.-P. Hansen and H. Löwen, *Annu. Rev. Phys. Chem.* **51**, 209 (2000).
  - [2] S. Asakura and F. Oosawa, *J. Chem. Phys.* **22**, 1255 (1954).
  - [3] S. Asakura and F. Oosawa, *J. Polym. Sci.* **33**, 183 (1958).
  - [4] Y. Mao, M.E. Cates, and H.N.W. Lekkerkerker, *Physica A* **222**, 10 (1995).
  - [5] B. Götzelmann, R. Evans, and S. Dietrich, *Phys. Rev. E* **57**, 6785 (1998).
  - [6] B. Götzelmann *et al.*, *Europhys. Lett.* **47**, 398 (1999).
  - [7] M. Dijkstra, R. van Roij, and R. Evans, *Phys. Rev. E* **59**, 5744 (1999).
  - [8] R. Roth, R. Evans, and S. Dietrich, *Phys. Rev. E* **62**, 5360 (2000).
  - [9] R. Evans, in *Fundamentals of Inhomogeneous Fluids*, edited by D. Henderson (Marcel Dekker, New York, 1992).
  - [10] S. Melchionna and J.-P. Hansen, *Phys. Chem. Chem. Phys.* **2**, 3465 (2000).
  - [11] Y. Rosenfeld, *J. Chem. Phys.* **98**, 8126 (1993).
  - [12] L.J.D. Frink and A.G. Salinger, *J. Comput. Phys.* **159**, 407 (2000); **159**, 425 (2000).
  - [13] T. Biben, P. Bladon, and D. Frenkel, *J. Phys.: Condens. Matter* **8**, 10 799 (1996).
  - [14] Y. Rosenfeld, *Phys. Rev. Lett.* **63**, 980 (1989).
  - [15] See, for example, J. -P. Hansen and I. R. McDonald, *Theory of Simple Liquids* (Academic Press, London, 1986), 2nd ed.
  - [16] Y. Rosenfeld, M. Schmidt, H. Löwen, and P. Tarazona, *Phys. Rev. E* **55**, 4245 (1997).
  - [17] D. Goulding, S. Melchionna, and J.-P. Hansen, *Phys. Rev. Lett.* **85**, 1132 (2000).
  - [18] R. Roth, and S. Dietrich, *Phys. Rev. E* **62**, 6926 (2000).
  - [19] D. Goulding, S. Melchionna, and J.-P. Hansen, *Phys. Chem. Chem. Phys.* **3**, 1644 (2001).
  - [20] D. Goulding and J.-P. Hansen, *Mol. Phys.* **99**, 865 (2001).
  - [21] D. Goulding, Ph.D. thesis, Cambridge University, 2000.
  - [22] P. Attard, *J. Chem. Phys.* **91**, 3083 (1989).